Polyhedron 242 (2023) 116495

Contents lists available at ScienceDirect

Polyhedron

journal homepage: www.elsevier.com/locate/poly

Chloromanganese and oxo-Titanium (IV) phthalocyanines: Synthesis, electrochemistry and Spectroelectrochemistry

Gülsev Dilber [a], Asiye Nas [a,*], Özlem Budak [b], Atıf Koca [b]

[a] Macka Vocational School, Karadeniz Technical University, 61750, Maçka, Trabzon, Turkey
[b] Department of Chemical Engineering, Engineering Faculty, Marmara University, İstanbul, Turkey

ARTICLE INFO

Keywords:
Electrochemistry
Spectroelectrochemistry
Manganese
Titanium dioxide
Phthalocyanine

ABSTRACT

Electrochemical properties of MPcs were determined with electrochemical and in-situ spectroelectrochemical measurements to investigate the influence of the metal center and the number and positions of the substituents. While H_2Pc only illustrated *Pc* based redox processes, the incorporation of TiO_2^+ and Cl^{-1}-Mn^{3+} cations into the cavity of *Pc* ring considerably altered the redox richness of the complexes. Two metal-based reduction couples were observed in addition to the *Pc*-based processes for both of TiOPc and MnPc. Moreover, altering the number and position of 4-(2-phenylpropan-2-yl)phenoxy substituents slightly influenced the basic redox activity of *Pc* ring and metal centers. All of these results supported the proposed structure of the complexes. During the redox reactions, pronounced spectral changes were observed with the in situ spectroelectrochemical measurements which caused distinct color changes. Rich redox responses and pronounced spectral and color changes of the complexes indicated their worth as functional material in various electrochemical technologies.

1. Introduction

It is well documented in the literature that a phthalocyanine (*Pc*) ring can give four reduction and two oxidation reactions and these redox responses can be modulated by the coordination of redox-active metal cations with the *Pc* ring and adding of redox-active substituents to the peripheral and/or nonperipheral positions of the *Pc* ring [1–3]. Moreover, the electron donating or withdrawing properties of the substituents and their positions and numbers were used to set the redox couples to the desired potentials [3]. All of these modifications were generally applied to obtain the desired redox activity for the proposed electrochemical applications [4–12]. For these purposes, numerous MPcs were reported, which have different metal centers and substituent environments. Here we have reported the synthesis and detailed electrochemistry of novel MPcs having H^+, TiO_2^+ and Cl^{-1}-Mn^{3+} central ions and eight and four 4-(2-phenylpropan-2-yl)phenoxy substituents on peripheral and/or nonperipheral positions of the *Pc* ring. TiO_2^+ and Cl^{-1}-Mn^{3+} cations were preferred due to their reduction activities and 4-(2-phenylpropan-2-yl)phenoxy substituents were chosen due to their electron donating the ability. These substituents have also ability to facilitate also the solubility of the complexes in various organic solvents.

2. Experimental

2.1. Materials

$MnCl_2$ (97%, Merck), *n*-pentanol (98%, Merck, Germany), 1.8-diazabisiklo[5.4.0]undek-7-en (DBU) (98%, Merck, India), $CHCl_3$ (99.8 %, Kimetsan, Turkey), CH_3OH (99%, Symras, Turkey), hexane (95%, Merck), silica gel (Merck, Germany), titanium (IV) butoxide (98%, Acros Organics, India). **1**–**4** were synthesized in a similar method reported in the literature using 4-cumylphenol (99%, Aldrich, USA) and 4-nitro phthalonitrile (99%, Acros Organics, China)/3-nitro phthalonitrile (98%, ABCR) /4,5-dichlorophthalonitrile (Chem Cruz) [13–14], 4,5-bis (4-(2-phenylpropan-2-yl)phenoxy)phthalonitrile starting materials [15]. Column chromatography was performed on silica gel 60 (particle size: 0.04–0.063 mm) for purification of the target compounds. The used reagents and solvents were dried and purified, as described in Perrin and Armarego before use [16].

2.2. Synthesis

2.2.1. Synthesis of four peripheral substituted Mn(III) phthalocyanine (5)

A mixture of 4-(4-(2-phenylpropan-2-yl)phenoxy)phthalonitrile (**2**)

* Corresponding author.
E-mail address: asiyenas@ktu.edu.tr (A. Nas).

https://doi.org/10.1016/j.poly.2023.116495
Received 6 February 2023; Accepted 5 June 2023
Available online 9 June 2023

(0.30 g, 0.87 mmol), anhydrous $MnCl_2$ (57 mg, 0.45 mmol), 3 drops of 1,8-diazabicyclo[5.4.0]undec-7-ene (DBU) in 4 mL of *n*-pentanol was heated to 160 ℃ with stirring for 24 h under nitrogen atmosphere. At the end of the time, hexane was added to the mixture cooled room temperature, the precipitated green product was filtered and dried in vacuum. The raw product was purified in a silica gel-loaded column using a $CHCl_3$:CH_3OH (93:7) solvent system. The solvent was evaporated to dryness in the evaporator, the resulting brown product was dried in the vacuum desiccator. Yield: 160 mg (50 %), m.p.: >300 °C. $C_{92}H_{72}N_8O_4MnCl$, FT-IR ν_{max}/cm^{-1}: 3054–3027 (Ar-H), 2964–2921 (Aryl-H), 1724, 1598, 1465, 1334, 1229 (Ar—O—C), 1071, 952, 762, 697, 566. MALDI-TOF, *m/z*: Calc.: 1444,03; Found: 1409,921 $[M-Cl+H]^+$. UV/vis (chloroform): λ, nm (log ε): 389 (4,88), 528 (4,49); 660 (4,60); 730 (5,26).

2.2.2. Synthesis of Non-Peripheral substituted Mn(III) phthalocyanine (6)

Synthesis of non-peripheral substituted Mn(III) phthalocyanine (**6**) was performed by a similar procedure to the synthesis of compound **5**. 3-(4-(2-phenylpropan-2-yl)phenoxy)phthalonitrile (**3**) (0.30 g, 0.87 mmol) and $MnCl_2$ (57 mg, 0.45 mmol) were used in this synthesis. The raw product was purified in a silica gel-loaded column using a $CHCl_3$:CH_3OH (87:13) solvent system. Yield: 57 mg (18 %), m.p.: >300 °C. $C_{92}H_{72}N_8O_4MnCl$, FT-IR ν_{max}/cm^{-1}: 3060–3029 (Ar-H), 2964–2923 (Aryl-H), 1771, 1714, 1587, 1473, 1327, 1246 (Ar—O—C), 1059, 986, 826, 743, 699. MALDI-TOF, *m/z*: Calc.: 1444,03; Found: 1407,977 $[M-Cl]^+$. UV/vis (chloroform): λ, nm (log ε): 342 (4,92), 535 (4,40); 678 (4,53); 755 (5,21).

2.2.3. Synthesis of eight peripheral substituted Mn(III) phthalocyanine (7)

Synthesis of eight-substituted Mn(III) phthalocyanine (**7**) was performed by a similar procedure to the synthesis of compound **5**. 4,5-bis(4-(2-phenylpropan-2-yl)phenoxy)phthalonitrile (**4**) (0.30 g, 0.55 mmol) and $MnCl_2$ (35 mg, 0.28 mmol) were used in this synthesis. The raw product was purified in a silica gel-loaded column using a $CHCl_3$:CH_3OH (87:13) solvent system.Yield: 108 mg (35 %), m.p.: >300 °C. $C_{152}H_{128}N_8O_8MnCl$, FT-IR ν_{max}/cm^{-1}: 3028 (Ar-H), 2964–2930 (Aryl-H), 1728, 1598, 1501, 1439, 1394, 1244 (Ar—O—C), 1070, 1014, 884, 743, 697. MALDI-TOF, *m/z*: Calc.: 2285,13; Found: 1718,39 $[M-3C_{15}H_{16}+Na\text{-}1]^+$, 1543,47 $[M-4C_{15}H_{16}-Cl+K+Na+H_2O\text{-}1]^+$. UV/vis (chloroform): λ, nm (log ε): 388 (4,98), 516 (4,52); 655 (4,66); 729 (5,32).

2.2.4. Synthesis of four peripheral substituted TiO phthalocyanine (8)

A mixture of 4-(4-(2-phenylpropan-2-yl)phenoxy)phthalonitrile (**2**) (0,20 g, 0,65 mmol), titanium (IV) butoxide (0,22 mL, 0,65 mmol), 3 drops of 1,8-diazabicyclo[5.4.0]undec-7-ene (DBU) in 2 mL of *n*-pentanol was heated to 160 ℃ with stirring for 24 h under nitrogen atmosphere. At the end of the time, hexane was added to the mixture cooled room temperature, the precipitated green product was filtered and dried in vacuum. Yield: 80 mg (38 %), m.p.: >300 °C. $C_{92}H_{72}N_8O_5Ti$, FT-IR ν_{max}/cm^{-1}: 3056–3027 (Ar-H), 2964–2930 (Aryl-H), 1741, 1599, 1472, 1362, 1227 (Ar—O—C), 1067, 946, 761, 697. MALDI-TOF, *m/z*: Calc.: 1417,51; Found: 1417,590 $[M]^+$. UV/vis (chloroform): λ, nm (log ε): 345 (4,87); 394 (4,53); 632 (4,60); 666 (4,77); 701 (5,23).

2.2.5. Synthesis of Non-Peripheral substituted TiO phthalocyanine (9)

Synthesis of non-peripheral substituted TiO phthalocyanine (**9**) was performed by a similar procedure to the synthesis of compound **8**. 3-(4-(2-phenylpropan-2-yl)phenoxy)phthalonitrile (**3**) (200 mg, 0,6 mmol) and titanium (IV) butoxide (0,10 mL, 0,3 mmol) were used in this synthesis.Yield: 18 mg (9 %), m.p.: >300 °C. $C_{92}H_{72}N_8O_5Ti$, FT-IR ν_{max}/cm^{-1}: 3055 (Ar-H), 2962–2925 (Aryl-H), 1618, 1484, 1330, 1238, 1131, 1056, 976, 802, 774, 632. MALDI-TOF, *m/z*: Calc.: 1417,51; Found: 1417,75 $[M]^+$. UV/vis (chloroform): λ, nm (log ε): 337 (4,89); 653 (4,65); 685 (4,83); 721 (5,26).

2.2.6. Synthesis of eight peripheral substituted TiO phthalocyanine (10)

Synthesis of eight-substituted TiO phthalocyanine (**10**) was performed by a similar procedure to the synthesis of compound **8**. 4,5-bis(4-(2-phenylpropan-2-yl)phenoxy)phthalonitrile (**4**) (200 mg, 0,36 mmol) and titanium (IV) butoxide (0,12 mL, 0,36 mmol) were used in this synthesis.Yield: 36 mg (18 %), m.p.: >300 °C. $C_{152}H_{128}N_8O_9Ti$, FT-IR ν_{max}/cm^{-1}: 3058 (Ar-H), 2960–2923 (Aryl-H), 1602, 1436, 1325, 1260, 1170, 1079, 995, 894, 747, 697. MALDI-TOF, *m/z*: Calc.: 2258,62; Found: 1905,04 $[M-2C_{15}H_{16}+K]^+$, 1730,75 $[M-3C_{15}H_{16}+K+Na\text{-}1]^+$, 1554,46 $[M-4C_{15}H_{16}+K+Na+H_2O+1]^+$, 1491,46 $[M-4C_{15}H_{16}+H_2O]^+$. UV/vis (chloroform): λ, nm (log ε): 349 (4,93); 632 (4,62); 700 (5,27); 667 (4,76).

2.3. Voltammetric and in situ spectroelectrochemical measurements

Cyclic voltammetric (CV) and square wave voltammetric (SWV) and spectroelectrochemical measurements were performed by using a Gamry Reference 600 Potentiostat/Galvanostat (Gamry Instruments in Louis Drive Warminster, USA) in an electrochemical cell having glassy carbon (GCE), platinum wire and Ag/AgCl working, counter and reference electrodes respectively in dimethyl sulfoxide (DMSO)/ tetrabutylammonium perchlorate (TBAP) electrolyte. Platinum (Pt) Mesh Electrode was used for in situ spectroelectrochemical (*SEC*) and in-situ spectrochronocoulometric (SCC) measurements in homemade thin layer quartz cell by using a Reference 600 Gamry potentiostat and OceanOptics diode array spectrophotometer (QE65000) (Ocean Optics in Geograaf 24, Duiven, The Netherlands). All of these measurements were performed by following the procedure published in the literature [17,18].

3. Results and discussion

3.1. Synthesis and characterization

The synthesis of nitrile 4-(4-(2-phenylpropan-2-yl)phenoxy)phthalonitrile (**2**)/3-(4-(2-phenylpropan-2-yl)phenoxy)phthalonitrile (**3**) and dinitrile compounds 4,5-bis(4-(2-phenylpropan-2-yl)phenoxy)phthalonitrile (**4**) used in the synthesis of manganese chloride and titanium oxide phthalocyanine compounds is available in the literature and they were synthesized again by following those methods. Compounds **2**–**4** were prepared by K_2CO_3 catalyzed nucleophilic aromatic nitro displacement of 4-nitrophthalonitrile/3-nitro phthalonitrile/4,5-dichlorophthalonitrile with 4-cumylphenol in DMF under N_2 atmosphere at 50 °C according to reported procedures [13–14]. The eight-substituted metal-free phthalocyanine compound (**1**) was synthesized in a study available in the literature [15], and its electrochemical properties were investigated in this study. The general synthetic route for the synthesis of novel manganese chloride and titanium oxide phthalocyanines is given in Scheme 1.

Compounds **5** and **8** showed very similar FT-IR absorptions to compound **2**, compounds **6** and **9** to compound **3**, and compounds **7** and **10** to compound **4**. The disappearance of the —C≡N band at 2233 cm^{-1}, 2229 cm^{-1} and 2243 cm^{-1}, respectively, after the formation of the phthalocyanine ring is evidence of cyclotetramerization of the dinitrile compound in the FT-IR spectrum.

Mass spectra were measured by the MALDI-TOF technique. The molecular ionic peaks of manganese phthalocyanines were observed at *m/z*: 1409,921 as $[M-Cl+H]^+$ for **5**, 1407,977 as $[M-Cl]^+$ for **6**, 1543,47 as $[M-4C_{15}H_{16}-Cl+K+Na+H_2O\text{-}1]^+$ for **7**, respectively. The molecular ionic peaks of titanium phthalocyanines were observed at *m/z*: 1417,590 as $[M]^+$ for **8**, 1417,75 as $[M]^+$ for **9**, 1491,46 as $[M-4C_{15}H_{16}+H_2O]^+$ for **10**, respectively. The MALDI-TOF mass spectra of phthalocyanines **5**–**10** contain intense molecular ion peaks with the weaker fragmentation peaks of the latter formed by cleavage of the bonds of a substitute group.

The electronic spectra of phthalocyanines show several bands

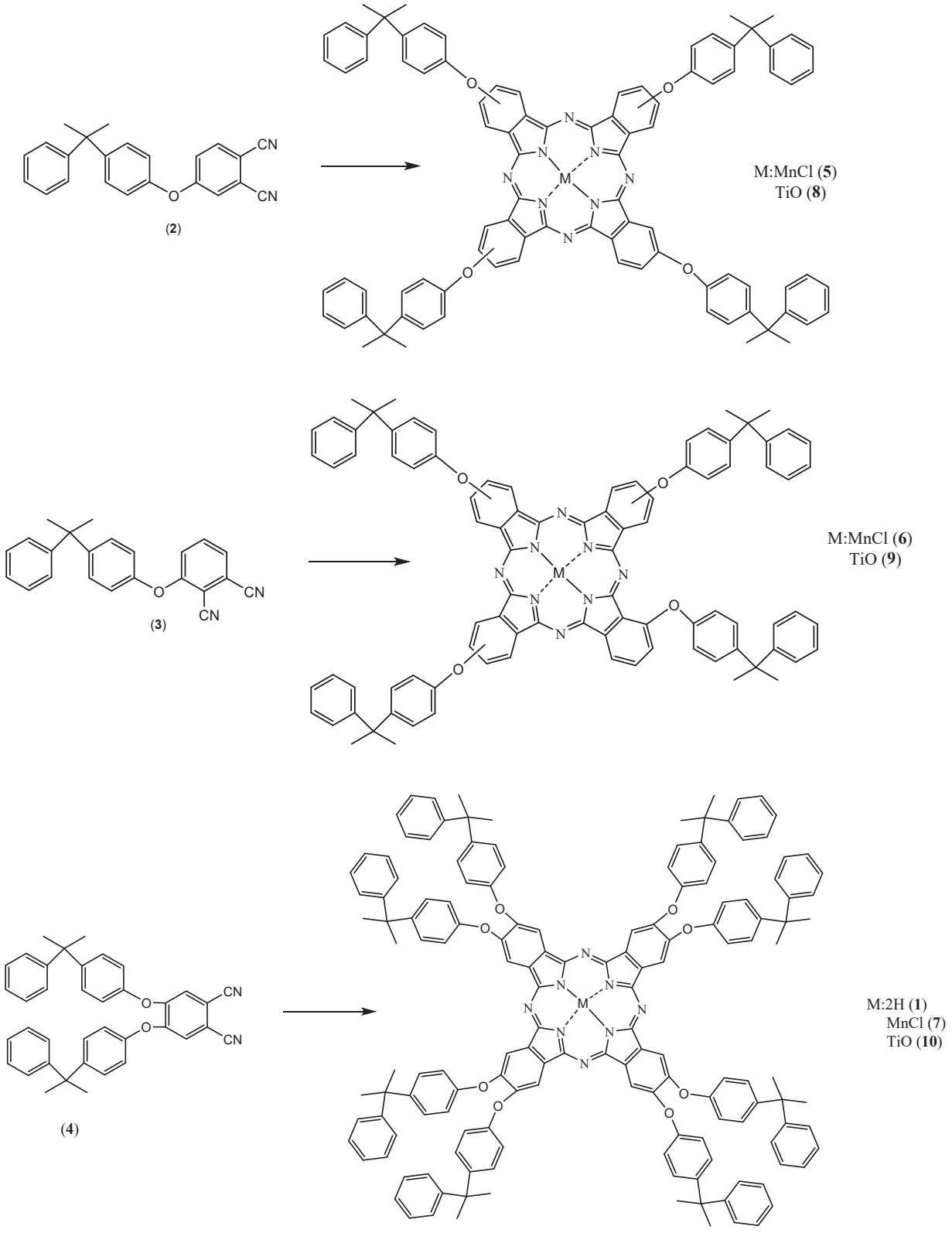

Scheme 1. Synthesis of four and eight peripheral substituted phthalocyanines (**1**, **5**–**10**).

resulting from π–π* and n–π* transitions. In the near UV there is a B band or Soret band between about 300–400 nm and there is the strongest Q band at about 600–700 nm. The Q bands of metal-free phthalocyanines appear as two bands divided into Qx and Qy bands due to the D_{2h} symmetry and degeneration of the LUMO (eg) level. In the UV spectrum of metalophthalocyanines, a single intense band is observed due to the D_{4h} symmetry [19]. Fig. 1 shows the UV–vis absorption spectra of complexes **5**–**10** in chloroform. Table 1 gives a summary of the Q band maxima of the manganese and titanium phthalocyanines (**5**–**10**). In UV–Vis spectra of the MnCl phthalocyanines (**5**–**7**) gave an intense single Q band absorption of the π–π* transitions at 730 nm for **5**, 755 nm for **6**, 729 nm for **7** with shoulders 660 and 528 nm for **5**; 678 and 535

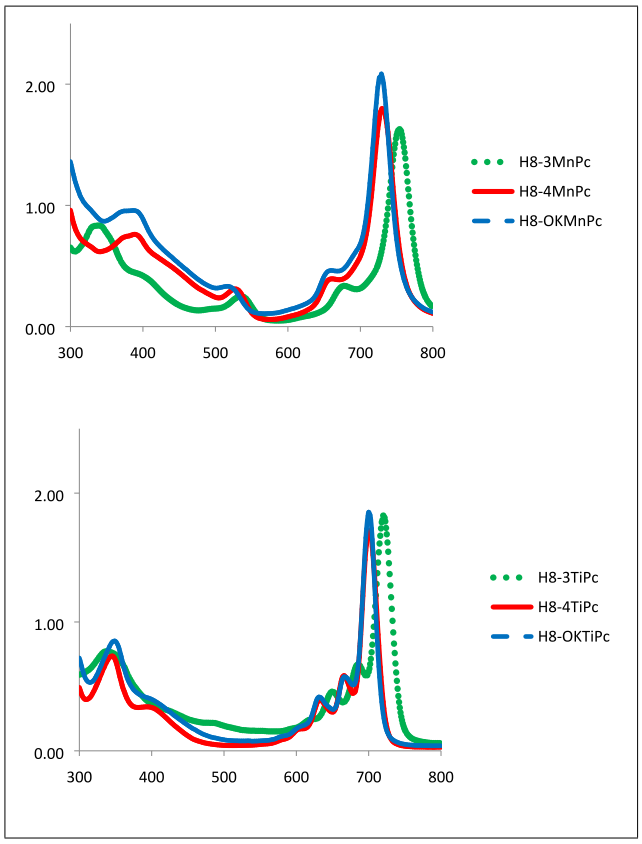

Fig. 1. UV–Vis electronic absorption spectra of the metallophthalocyanines in chloroform at 1.00×10^{-5} M.

Table 1
UV–Vis electronic absorption spectral data of the metallophthalocyanines in chloroform at 1.00×10^{-5} M.

	Solvent	Q band, λmax (nm)	log ε	B band, λmax (nm)	log ε
MnClPc (5)	Chloroform	730	5, 26	528	4,49
		660	4,60	389	4,88
MnClPc (6)	Chloroform	755	5,21	535	4,40
		678	4,53	342	4,92
MnClPc (7)	Chloroform	729	5,32	516	4,52
		655	4,66	388	4,98
TiOPc (8)	Chloroform	701	5,23	394	4,53
		666	4,77	345	4,87
		632	4,60		
TiOPc (9)	Chloroform	721	5,26	337	4,89
		685	4,83		
		653	4,65		
TiOPc (10)	Chloroform	700	5,27	349	4,93
		667	4,76		
		632	4,62		

nm for **6**; 655 and 516 nm for **7**; respectively. The B bands of complex were observed at 389 nm for **5**, 342 nm for **6** and 388 nm for **7**, respectively. The UV–Vis spectra of the TiO phthalocyanines (**8**–**10**) gave an intense single Q band absorption of the π-π* transitions at 701 nm for **8**, 721 nm for **9**, 700 nm for **10** with shoulders 666 and 632 nm for **8**; 685 and 653 nm for **9**; 667 and 632 nm for **10**; respectively. The B bands of complex were observed at 394 and 345 nm for **8**, 337 nm for **9** and 349 nm for **10**, respectively.

3.2. Electrochemical characterizations

Electrochemical characterization studies were performed on GCE in DMSO/TBAP electrolyte. With the analyses of the recorded voltammograms, the half wave potentials ($E_{1/2}$) were derived, and they are tabulated in Table 2. In order to investigate the central metal effects on the redox properties, the voltammetric responses of H_2Pc, TiOPc and MnPc complexes were determined and compared with each others. Fig. 2 represents CVs and SWVs of H_2Pc (**1**), which illustrates three reduction and two oxidation reactions within the potential window of the DMSO/TBAP electrolyte.While well-defined and clear reduction couples are observed at −0.57, −0.84, and −1.67 V, the oxidation reactions at 1.05 V and 1.34 V are complicated with possible preceding chemical reactions. Especially the first broad anodic wave at around 1.05 V resultes from aggregation of the complex, and oxidation of the aggregated and nonaggregated species reflects a complex redox response. $_{\Delta Ep}$ and I_{pa}/I_{pc} values of the redox couples indicate that while the first and second reduction couples are electrochemically and chemically reversible, remaining processes have chemically irreversible characters. When compared with the similar H_2Pc type complexes in the literature, redox processes of H_2Pc slightly shift towards the positive potentials due to the electron donating ability of the 4-(2-phenylpropan-2-yl)phenoxy substituents. Moreover, the positions and number of redox couples are in agreement with the reported ones [3,20–22].

It is reported in the literature that the redox mechanism of TiOPc complexes is considerably different than that of other MPcs. MPcs having redox active metal centers generally give metal-based reduction processes before the *Pc* ones. However, the first reduction peak is observed in advance and then the second reduction processes of TiOPc (**10**) are observed between the *Pc* based reduction reactions [23–26]. As shown in Fig. 3, redox responses of TiOPc studied here are in agreement with the similar TiOPcs in the literature [23–26]. The analysis of the voltammograms and the spectral changes discussed below shows the mechanism given in Eq. (1). As shown in the mechanism, R_1 and R_3 couples are assigned to the metal based reductions while all others are *Pc* based electron transfer reactions. While all reduction couples are almost electrochemically and chemically reversible with respect to $_{\Delta Ep}$ and I_{pa}/I_{pc} values, both of the oxidation couples are chemically irreversible.

$$\left[TiO^{2+}Pc^{1-}\right] \overset{E_{1/2}=1.38\ V}{\underset{O_2}{\Leftrightarrow}} \left[TiO^{2+}Pc^{0}\right]^{2+}$$

$$\left[TiO^{2+}Pc^{2-}\right] \overset{E_{1/2}=1.17\ V}{\underset{O_1}{\Leftrightarrow}} \left[TiO^{2+}Pc^{1-}\right]^{1+}$$

$$\left[TiO^{2+}Pc^{2-}\right] \overset{E_{1/2}=-0.49\ V}{\underset{R_1}{\Leftrightarrow}} \left[TiO^{1+}Pc^{2-}\right]^{1-}$$

$$\left[TiO^{1+}Pc^{2-}\right]^{1-} \overset{E_{1/2}=-0.66\ V}{\underset{R_2}{\Leftrightarrow}} \left[TiO^{1+}Pc^{3-}\right]^{2-}$$

$$\left[TiO^{1+}Pc^{3-}\right]^{2-} \overset{E_{1/2}=-0.82\ V}{\underset{R_3}{\Leftrightarrow}} \left[TiOPc^{3-}\right]^{3-}$$

$$\left[TiOPc^{3-}\right]^{3-} \overset{E_{1/2}=-1.00\ V}{\underset{R_4}{\Leftrightarrow}} \left[TiOPc^{4-}\right]^{4-}$$

$$\left[TiOPc^{4-}\right]^{4-} \overset{E_{1/2}=-1.70\ V}{\underset{R_5}{\Leftrightarrow}} \left[TiOPc^{5-}\right]^{5-}$$

Fig. 4 illustrates the CV and SWV responses of MnPc (**7**), which gives three reduction and two oxidation processes. The main difference of MnPc to the previous H_2Pc and TiOPc is the observation of the first reduction process at around 0 V (R1 process at −0.03 V). It is well known that this process is associated to the reduction of the central metal cation, thus it is assigned to the $[Cl^{1-}\text{-}Mn^{III}Pc^{2-}]/[Cl^{1-}\text{-}Mn^{II}Pc^{2-}]^{1-}$ process. In situ spectroelectrochemical results given below support this assignment. There is a disagreement in the literature on the assignments of the second reduction process of MnPc complexes. While some papers assigned it to a *Pc* based reduction, others assigned to metal-based reduction reactions [5,19,27–30]. It is clear that if the potential

Table 2
Electrochemical data of the complexes in DMSO/TBAP solution. All potentials were given versus Ag/AgCl.

Complexes	$E_{1/2}$ (V) of Redox Processes R_1	R_2	R_3	R_4	O_1	O_2	Ref.
H_2Pc (**1**)	−0.57	−0.84	−1.67		1.05	1.34	tw
MnClPc (**5**)	−0.12 (-0.37)	−0.81 (-1.22)	−1.42 (-1.62)		1.04	1.36	Tw
MnClPc (**6**)	0.03 (-0.22)	−0.79	−1.22		0.82	1.23	Tw
MnClPc (**7**)	−0.03	−0.73	−1.13 (-1.30)		0.63	1.18	Tw
TiOPc (**10**)	−0.49	−0.66	−0.82	−1.00 (-1.70)	1.17	1.38	Tw
H2Pca	−0.78	−1.30	−1.90		0.93	1.14	[3]
H2Pca	−0.80	−1.23	−1.47		0.94	1.23	[3]
H2Pca	−0.83	−1.13	–		0.82	–	[43]
TiOPcb	−0.48	−0.63	−0.83	−0.99 (1.70)	0.80	–	[22]
TiOPcb	−0.47	−0.62	−0.81	−0.96 (1.35)	0.96	–	[22]
TiOPca	−0.73	–	−1.09	–	0.54	0.94	[24]
MnPca	−0.26	−0.98	–		0.30	0.83	[24]
MnClPca	−0.30	−0.90	−1.36		0.38 (0.51)	0.88	[44]
MnTMPyrPc	−0.06	−0.68	−1.19		–	–	[45]
MnClPc(m)	−0.23	−0.80	−1.04		–	–	[46]

a: $E_{1/2}$ values were given versus SCE in DCM/TBAP electrolyte. [b]: $E_{1/2}$ values were given versus SCE in DMSO/TBAP electrolyte.

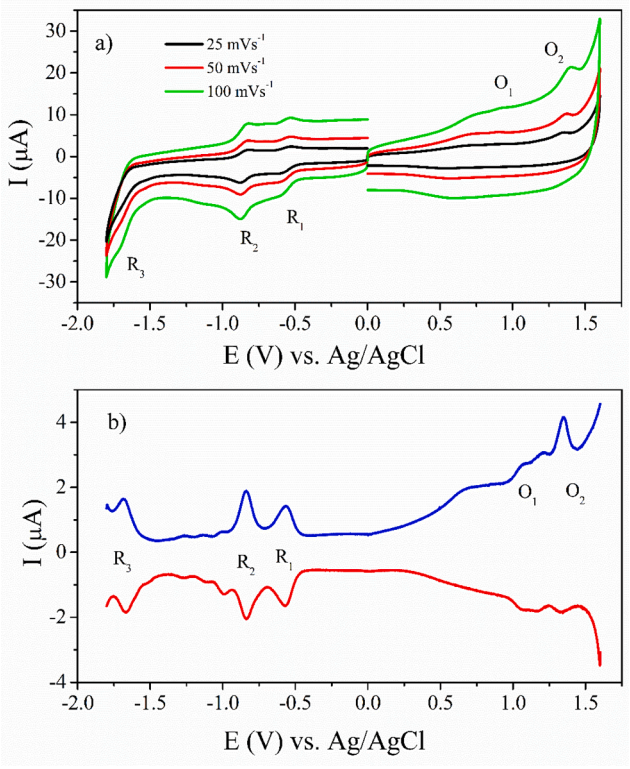

Fig. 2. Voltammograms of H_2Pc (**1**) (5.0×10^{-4} mol dm^{-3}) recorded at various scan rates on a GCE working electrode in DMSO/TBAP. a) CVs, b) CVs recorded with different switching potentials and c) SWVs.

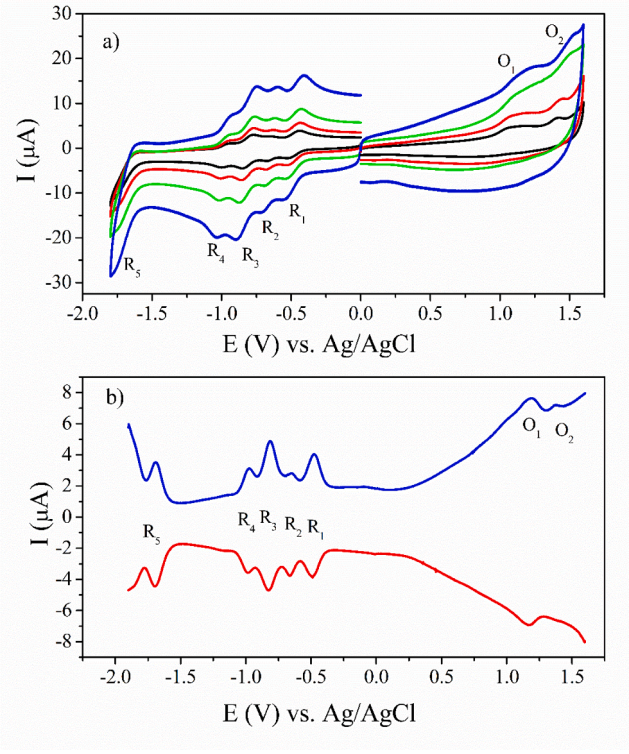

Fig. 3. Voltammograms of TiOPc (**10**) (5.0×10^{-4} mol dm^{-3}) recorded at various scan rates on a GCE working electrode in DMSO/TBAP. a) CVs, b) CVs recorded with different switching potentials and c) SWVs.

separation between the first and second reductions for MnPc is below 0.80 V, both of them are reported as metal-based processes. With respect to all these discussions, the second reduction couple R_2 (at −0.73 V) of MnPc studied here is easily assigned to $[Cl^{1-}\text{-}Mn^{II}Pc^{2-}]^{1-}/[Cl^{1-}\text{-}Mn^{I}Pc^{2-}]^{2-}$ process. Peak-to-peak separation (0.70 V) between R_1 of R_2 support this assignment. With respect to the comparisons with the similar papers in the literature, while the first two reduction couples are assigned to the metal-based processes, all other processes are assigned to the *Pc* ring based electron transfer reactions. This proposed mechanism is represented in Eq. 2. $_{\Delta Ep}$ and I_{pa}/I_{pc} analysis and the SWV responses of MnPc indicate chemical irreversibilities of the reduction processes. The nature of this irreversibility is analyzed with altering the vertex potentials of CVs. As shown in Fig. 5**a**, when the switching potentials shift just after the third reduction reaction, three reduction reactions are electrochemically and chemically reversible. However, when the vertex potential passes the fourth reduction reaction, all processes get chemically irreversible. These data indicate the presence of a chemical

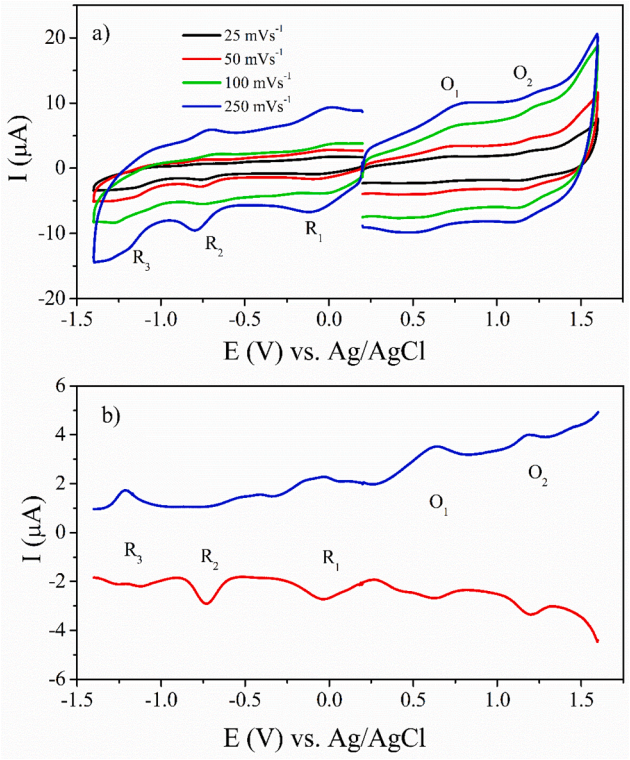

Fig. 4. Voltammograms of MnPc (**7**) (5.0 × 10^{-4} mol dm^{-3}) recorded at various scan rates on a GCE working electrode in DMSO/TBAP. a) CVs, b) CVs recorded with different switching potentials and c) SWVs.

reaction after the fort reduction process. Releasing of the axial Cl^{1-} ligand might be the occuring chemical reaction [5,31,32] and as a result of this, $\left[Cl^{1-}Mn^{1+}Pc^{4-}\right]^{4-}$ species are converted to $\left[Mn^{1+}Pc^{4-}\right]^{3-}$ species which make all processes chemically irreversible.

$$\left[Cl^{1-}Mn^{3+}Pc^{1-}\right]^{1+} \overset{E_{1/2}=1.18V}{\underset{O_2}{\Leftrightarrow}} \left[Cl^{1-}Mn^{3+}Pc^{0}\right]^{2+}$$

$$\left[Cl^{1-}Mn^{3+}Pc^{2-}\right] \overset{E_{1/2}=\ 0.63\ V}{\underset{O_1}{\Leftrightarrow}} \left[Cl^{1-}Mn^{3+}Pc^{1-}\right]^{1+}$$

$$\left[Cl^{1-}Mn^{3+}Pc^{2-}\right] \overset{E_{1/2}=-0.03\ V}{\underset{R_1}{\Leftrightarrow}} \left[Cl^{1-}Mn^{2+}Pc^{2-}\right]^{1-}$$

$$\left[Cl^{1-}Mn^{2+}Pc^{2-}\right]^{1-} \overset{E_{1/2}=-0.73\ V}{\underset{R_2}{\Leftrightarrow}} \left[Cl^{1-}Mn^{1+}Pc^{2-}\right]^{2-}$$

$$\left[Cl^{1-}Mn^{1+}Pc^{2-}\right]^{2-} \overset{E_{1/2}=-1.13\ V}{\underset{R_3}{\Leftrightarrow}} \left[Cl^{1-}Mn^{1+}Pc^{3-}\right]^{3-}$$

$$\left[Cl^{1-}Mn^{1+}Pc^{3-}\right]^{3-} \overset{E_{1/2}=-1.30\ V}{\underset{R_4}{\Leftrightarrow}} \left[Cl^{1-}Mn^{1+}Pc^{4-}\right]^{4-}$$

$$\left[Cl^{1-}Mn^{1+}Pc^{4-}\right]^{4-} \xrightarrow{chemical\ \ reaction} \left[Mn^{1+}Pc^{4-}\right]^{3-} + Cl^{1-}$$

In order to investigate the effects of the substituent number and their position, CV analysis of MnPcs having eight and nonperipherally and peripherally four substituents are carried out. As shown in Fig. 5**a**–**c**, while R_1–R_3 processes of MnPc (**7**) have electrochemically reversible characters, these processes are chemically irreversible due to the following chemical reactions. R1 of MnPc(np,3) and R1 and R2 of MnPc (per,4) split into two waves due to the succeeding chemical reactions. Moreover, reversing the vertex potential from more negative potentials influenced the chemical reversibility of the reduction processes for all

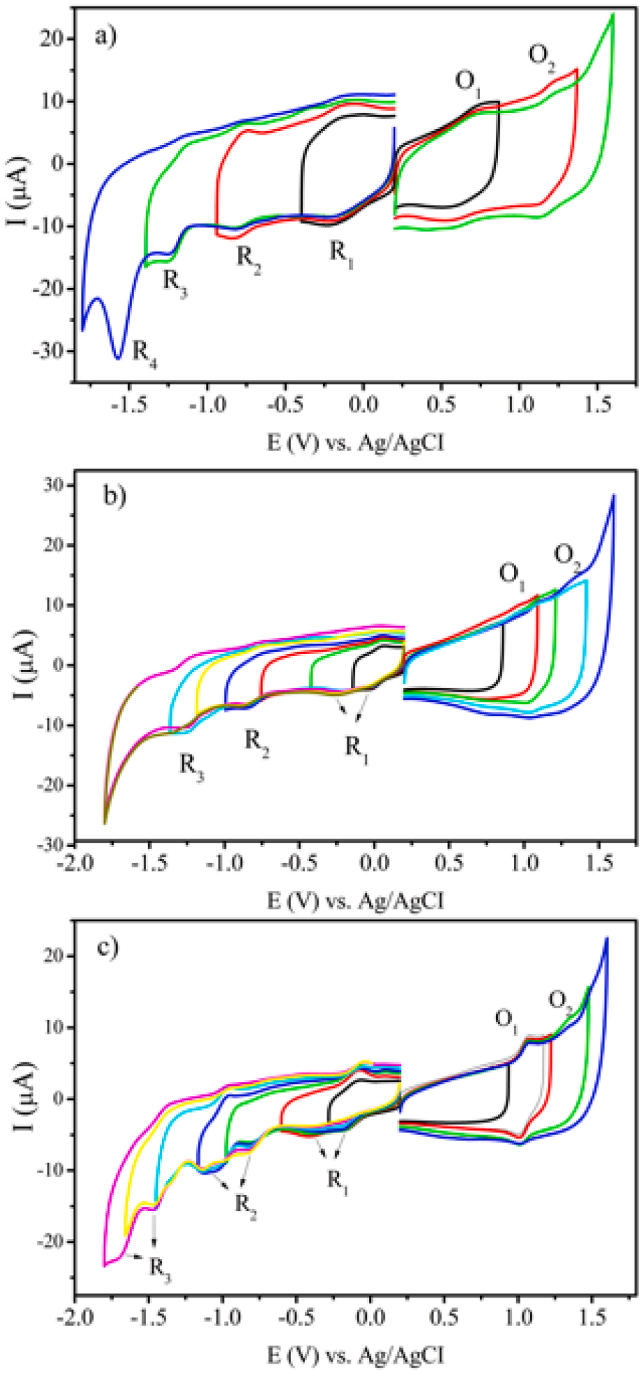

Fig. 5. CVs of MnPcs (5.0 × 10^{-4} mol dm^{-3}) recorded with various vertex potentials at 100 mVs^{-1} scan rate on a GCE working electrode in DMSO/TBAP. a) MnPc (**7**), b) MnPc (**6**), b) MnPc (**5**).

complexes. Altering the substituent on the MnPcs considerably influences the peak positions. When the complexes are compared with each other, it is observed that MnPc(np,3) is reduced more easily than MnPc(per,4) and therefore redox peaks of MnPc(np,3) are recorded at more positive potentials.

3.3. *In-Situ spectroelectrochemical measurements*

In-situ spectroelectrochemical (*SEC*) measurements are carried out to support the mechanism proposed using voltammetric measurements. Moreover, chromaticity diagrams are recorded to determine the color of the electrogenerated species of the complexes. H_2Pc (**1**) only shows *Pc*

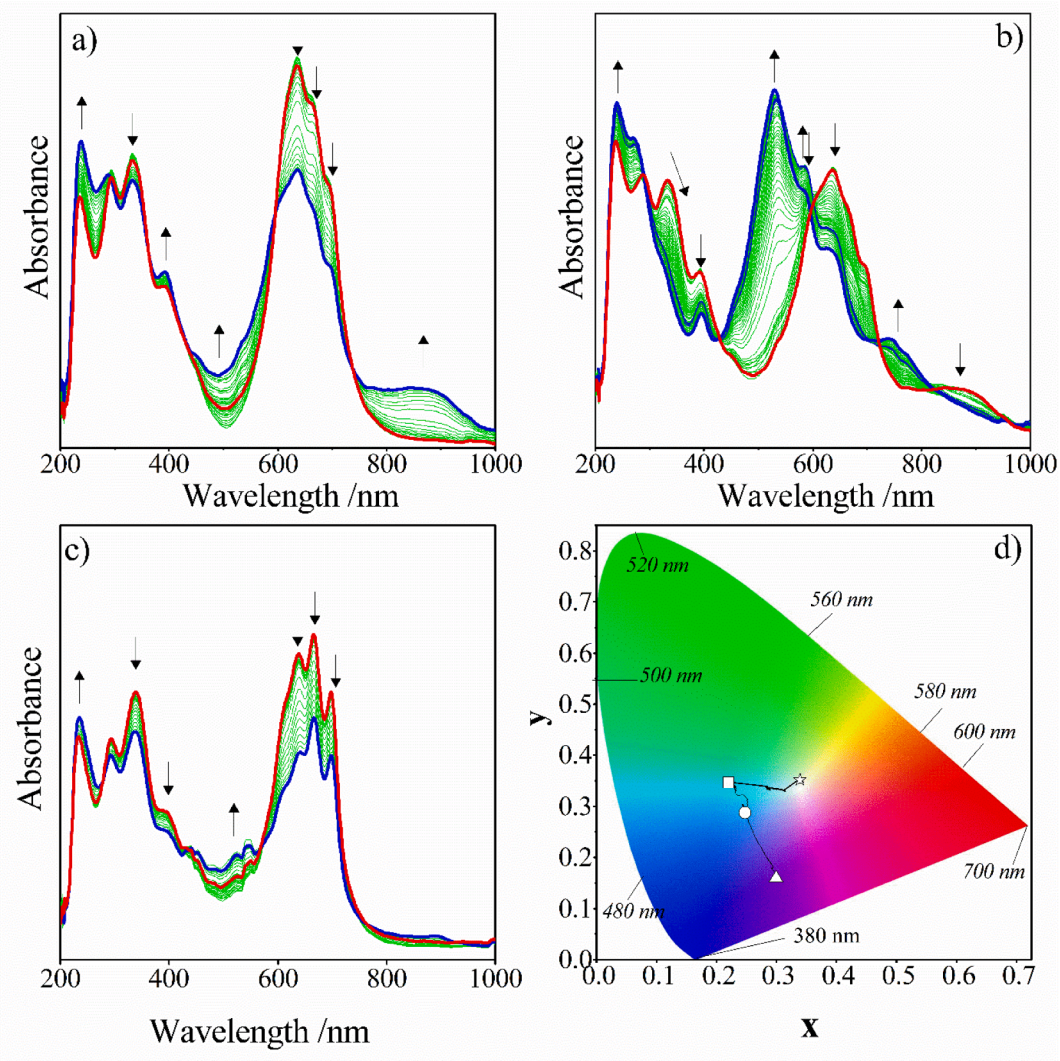

Fig. 6. In-situ UV–Vis spectral changes of H_2Pc (**1**) in DMSO/TBAP electrolyte. **a**) E_{app} = -0.70 V **b**) E_{app} = −1.20 V, **c**) E_{app} = 1.20 V, **d**) Chromaticity diagram (each symbol represents the color of electro-generated species; □: $[H_2Pc^{-2}]$; ○:$[H_2Pc^{-3}]^{1-}$; △: $[H_2Pc^{-4}]^{2-}$; *: $[H_2Pc^{-1}]^{1+}$.

ring based redox reactions thus, characteristic *Pc* based spectral changes are recorded during all redox reactions of H_2Pc as shown in Fig. 6 [30,33–35]. During the R_1 process of H_2Pc, the split Q bands at 666 and 696 nm and the aggregation band at 636 nm decrease in intensity without a shift and the absorption of charge transfer regions increases (Fig. 6**a**). This spectral change causes a color change from cyan (point x = 0.224 and y = 0.345) to light blue (point x = 0.247 and y = 0.308) as shown in the chromaticity diagram in Fig. 6**d**. These spectral responses are characteristic changes for the *Pc* reduction processes. During the second reduction process, while the Q band disappears completely a huge band is observed at 528 nm (Fig. 6**b**). The light blue color of the monoanionic H_2Pc species turns to deep blue (point x = 0.297 and y = 0.162) after the second reduction reaction (Fig. 6**d**). Similar spectral changes are observed during the oxidation of H_2Pc. The Q bands decrease, while a small band is observed at 525 nm (Fig. 6**c**). As a result of these spectral changes the cyan color turns to yellow for the cationic form of H_2Pc (Fig. 6**d**).

Spectroelectrochemical responses of TiOPc (**10**) are represented in Fig. 7. At −0.55 V applied potential, the Q band at 700 nm and a small new band at 684 nm increase slightly due to the reduction of $\left[TiO^{2+}Pc^{2-}\right]$ specie to $\left[TiO^{1+}Pc^{2-}\right]^{1-}$ species (Fig. 7**a**) [24,25,30,36]. Green color (point x = 0.280 and y = 0.411) of neutral $\left[TiO^{2+}Pc^{2-}\right]$ turn to bluish green (point x = 0.242 and y = 0.398) for the $\left[TiO^{1+}Pc^{2-}\right]^{1-}$ species after the first reduction reaction as shown in the chromaticity diagram. During the second reduction reaction the Q band decreases slightly while a new small band forms at 522 nm. These spectral changes cause of the color change from bluish-green to cyan (point x = 0.240 and y = 0.326). These spectral changes are in agreement with the *Pc* reduction of the complex. (Fig. 7**a** inset). Fig. 7**b** and its inset represent the spectral changes observed during the third and fourth reduction reactions. The spectral changes observed during the reduction reactions discussed above support the proposed peak assignments performed with voltametric measurements. During the oxidation reaction, all bands decrease in intensity due to the decomposition of the cationic form of the complex under applied positive potential (Fig. 7**c**). Pronounced color changes shown in the chromaticity diagram indicate possible usage of the complex in display technologies, such as electrochromic applications, data storage and optic diodes.

MnPc having eight and four substituents illustrate similar spectroelectrochemical responses thus the in-situ UV–Vis spectral changes of MnPc (**7**) in DMSO/TBAP electrolyte during the redox reactions are given in Fig. 8 as an example. In the neutral state, MnPc (**7**) gives the Q band at 726 nm and B bands at 288 and 394 nm. Moreover, the band which is characteristic for the Mn^{III} oxidation state is observed at 516 nm. Under

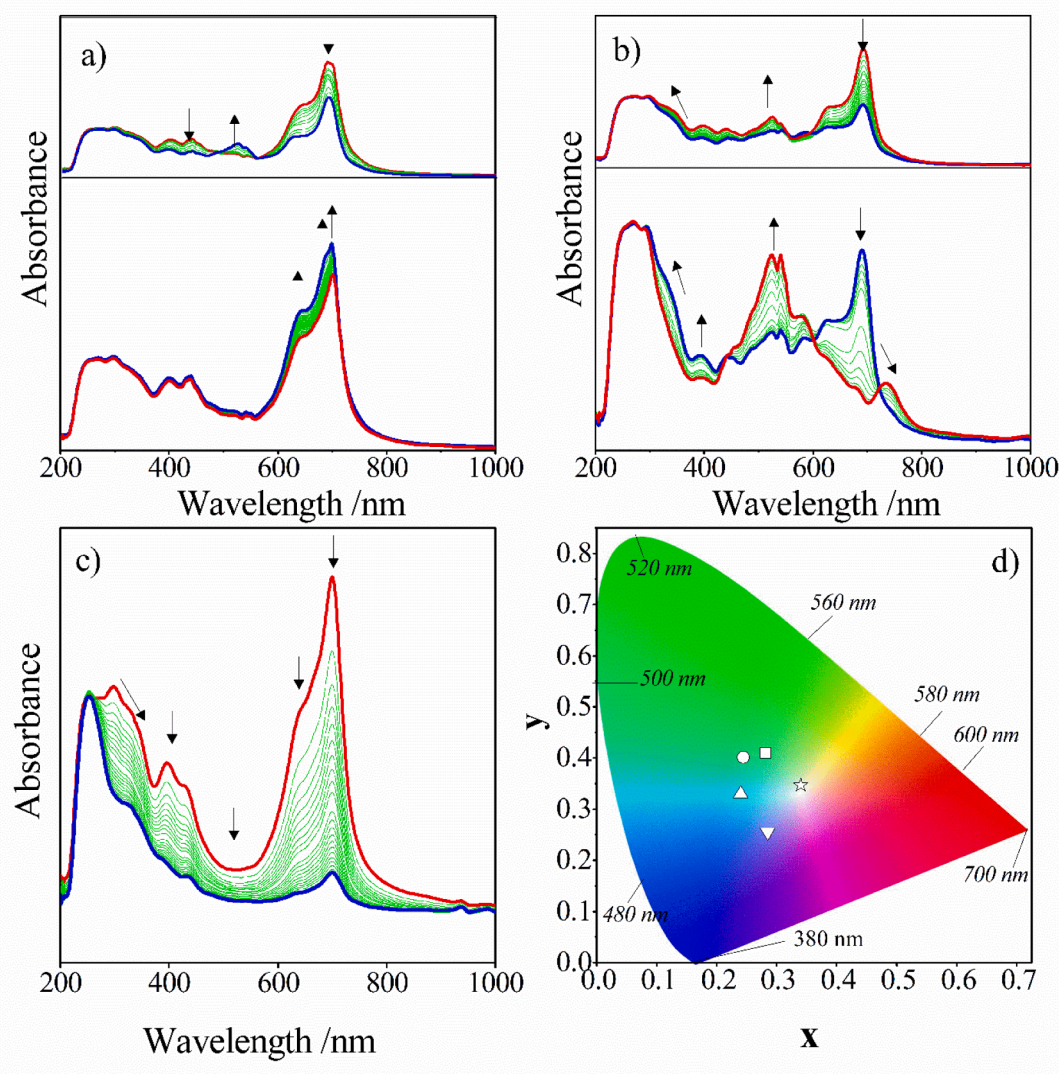

Fig. 7. In-situ UV–Vis spectral changes of TiOPc (**10**) in DMSO/TBAP electrolyte. **a**) E_{app} = -0.55 V (inset: E_{app} = -0.75 V). **b**) (inset: E_{app} = -0.90 V) E_{app} = -1.10 V, **c**) E_{app} = 1.25 V, **d**) Chromaticity diagram (each symbol represents the color of electro-generated species; □: [$TiO^{II}Pc^{-2}$]; ○:[$TiO^{I}Pc^{-2}$]$^{1-}$; △: [$TiO^{II}Pc^{-3}$]$^{2-}$; ▼: [$TiO^{I}Pc^{-3}$]$^{3-}$; *: [$TiO^{II}Pc^{-1}$]$^{1+}$.

−0.30 V applied potential, a new Q band which is characteristic for the Mn^{II} oxidation state is enhanced at 682 nm, while the Q band at 726 nm decreases in intensity (Fig. 8**a**). Moreover, the band at 516 nm decreases due to the conversion of the Mn^{III} to Mn^{II} state. These spectral changes confirm the proposed $\left[Cl^{1-}Mn^{3+}Pc^{2-}\right]/\left[Cl^{1-}Mn^{2+}Pc^{2-}\right]^{1-}$ mechanism for the first reduction reaction [26,30,37–42]. As a result of the reduction the orange color (point x = 0.395 and y = 0.386) of the neutral $\left[Cl^{1-}Mn^{3+}Pc^{2-}\right]$ species turns to yellow (point x = 0.356 and y = 0.371) $\left[Cl^{1-}Mn^{2+}Pc^{2-}\right]^{1-}$ (Fig. 8**d**). Fig. 8**b** (inset) shows the spectral changes under −0.90 V. A new characteristic band for the formation of $\left[Cl^{1-}Mn^{1+}Pc^{2-}\right]^{2-}$ species is formed at 615 nm, while the bands at 516 and 726 nm completely disappear. After this reduction reaction, color is changed to cyan (point x = 0.316 and y = 0.345) of the $\left[Cl^{1-}Mn^{1+}Pc^{2-}\right]^{2-}$ species. The spectral changes given in Fig. 8**b**, support the *Pc*-based assignments of the third reduction process. The enhanced bands at 542, 731 and 810 nm and decreasing the Q band without a shift are the characteristic changes for $\left[Cl^{1-}Mn^{1+}Pc^{2-}\right]^{2-}$ to $\left[Cl^{1-}Mn^{1+}Pc^{3-}\right]^{3-}$. Similarly, distinct color changes from cyan to blue (point x = 0.291 and y = 0.267) and then to purple (point x = 0.325 and y = 0.250) are observed after the third and fourth reduction reactions as shown in the chromaticity diagram in Fig. 8**d**. Decreasing the Q band and the appearance of new bands at 572 and 828 nm indicate oxidation of $\left[Cl^{1-}Mn^{3+}Pc^{2-}\right]$ to $\left[Cl^{1-}Mn^{3+}Pc^{1-}\right]^{1+}$ under 0.70 V applied potential (Fig. 8**d**). These spectral changes cause a color change to red (point x = 0.296 and y = 0.308). The dicationic form of MnPc decomposes thus all bands decrease in intensity under 1.30 V applied potential.

4. Conclusion

Voltammetric measurements indicated that the redox activity of *Pc* rings can be enhanced with the incorporation of redox-active TiO^{2+} and Mn^{3+} metal cations. Additional two metal-based reduction reactions of TiOPc and MnPc indicate their possible usage as active electrocatalyst for the reduction reactions, such as oxygen reduction reactions in fuel cells and metal-air batteries. Moreover, they can be used as active electrocatalyst for water-splitting reactions. In addition to the

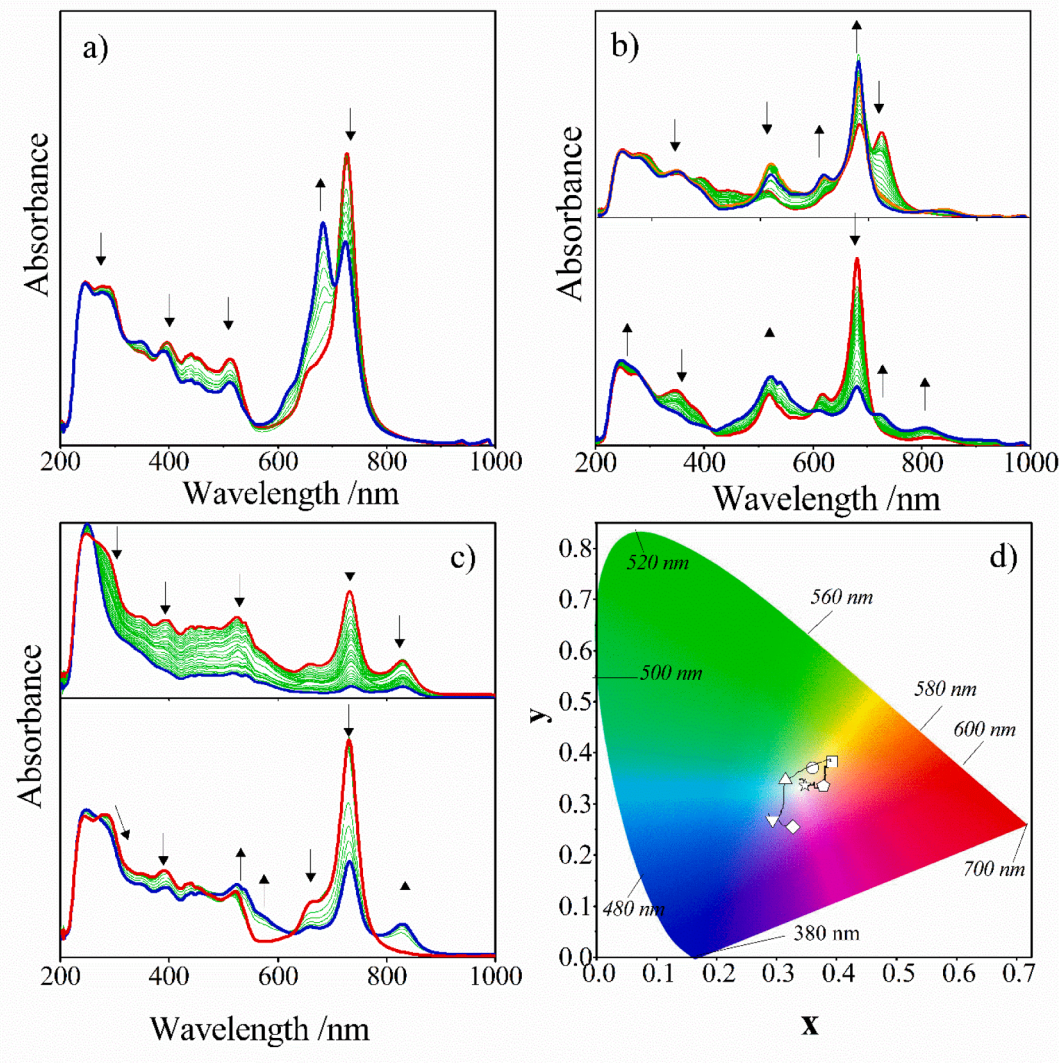

Fig. 8. In-situ UV–Vis spectral changes of MnPc (**7**) in DMSO/TBAP electrolyte. **a)** $E_{app} = -0.30$ V **b)** $E_{app} = -0.80$ V (inset: $E_{app} = -1.40$ V), **c)** $E_{app} = 0.80$ V, **d)** Chromaticity diagram (each symbol represents the color of electro-generated species; □: $[Cl^{1-}\text{-}Mn^{III}Pc^{-2}]$; ○:$[Cl^{1-}\text{-}Mn^{II}Pc^{-2}]^{1-}$; △: $[Cl^{1-}\text{-}Mn^{I}Pc^{-2}]^{2-}$; ▼: $[Cl^{1-}\text{-}Mn^{I}Pc^{-3}]^{3-}$; ◇: $[Cl^{1-}\text{-}Mn^{I}Pc^{-4}]^{4-}$;◆: $[Cl^{1-}\text{-}Mn^{III}Pc^{-1}]^{1+}$; *: $[Cl^{1-}\text{-}Mn^{III}Pc^{0}]^{2+}$.

voltammetric measurements, spectroelectrochemical characterizations were also used to determine the redox mechanisms and electrocolorimetric responses of the complexes. The in situ spectroelectrochemical results supported the proposed mechanisms for the electron transfer reactions of the complexes. The mechanisms for TiOPc and MnPc showed multielectron and metal and/or *Pc*-based redox activity of TiOPc and MnPc. The redox activity and distinct color differences between the electrogenerated complexes are some of the basic features of the functional materials for electrochemical technologies such as electrocatalysts, ptotosensitizers and electrochromophores.

Declaration of Competing Interest

The authors declare that they have no known competing financial interests or personal relationships that could have appeared to influence the work reported in this paper.

Data availability

No data was used for the research described in the article.

Acknowledgements

Atıf Koca thanks the Turkish Academy of Sciences (TUBA) for its support. This study was supported by the Research Fund of Karadeniz Technical University, Project no: FBA-2020-8426 (Trabzon-Turkey).

References

[1] M. L'her, A. Pondaven, Electrochemistry of 104, The Porphyrin Handbook (2003) 117.
[2] A. Lever, P. Minor, Electrochemistry of main-group phthalocyanines, Inorg. Chem. 20 (1981) 4015–4017.
[3] R. Li, X. Zhang, P. Zhu, D.K. Ng, N. Kobayashi, J. Jiang, Electron-donating or-withdrawing nature of substituents revealed by the electrochemistry of metal-free phthalocyanines, Inorg. Chem. 45 (2006) 2327–2334.
[4] K.I. Ozoemena, T. Nyokong, Surface electrochemistry of iron phthalocyanine axially ligated to 4-mercaptopyridine self-assembled monolayers at gold electrode: Applications to electrocatalytic oxidation and detection of thiocyanate, J. Electroanal. Chem. 579 (2005) 283–289.
[5] K.I. Ozoemena, T. Nyokong, Comparative electrochemistry and electrocatalytic activities of cobalt, iron and manganese phthalocyanine complexes axially co-ordinated to mercaptopyridine self-assembled monolayer at gold electrodes, Electrochim. Acta 51 (2006) 2669–2677.
[6] D. Akyüz, A. Koca, Construction of modified electrodes with click electrochemistry based on the hybrid of 4-azido aniline and manganese phthalocyanine and electrochemical pesticide sensor applications, J. Electrochem. Soc. 165 (11) (2018) B508–B514.

[7] D. Akyüz, A. Koca, An electrochemical sensor for the detection of pesticides based on the hybrid of manganese phthalocyanine and polyaniline, Sens. Actuat. B 283 (2019) 848–856.
[8] L.S. Koodlur, Layer-by-layer self assembly of a water-soluble phthalocyanine on gold. Application to the electrochemical determination of hydrogen peroxide, Bioelectrochemistry 91 (2013) 21–27.
[9] C. Solis, E. Baigorria, M.E. Milanesio, G. Morales, E.N. Durantini, L. Otero, M. Gervaldo, Electrochemical polymerization of EDOT modified Phthalocyanines and their applications as electrochromic materials with green coloration, and strong absorption in the Near-IR, Electrochim. Acta 213 (2016) 594–605.
[10] E. Jubete, K. Żelechowska, O.A. Loaiza, P.J. Lamas, E. Ochoteco, K.D. Farmer, K. P. Roberts, J.F. Biernat, Derivatization of SWCNTs with cobalt phthalocyanine residues and applications in screen printed electrodes for electrochemical detection of thiocholine, Electrochim. Acta 56 (2011) 3988–3995.
[11] E. Demir, H. Silah, B. Uslu, Phthalocyanine Modified Electrodes in Electrochemical Analysis, Crit. Rev. Anal. Chem. 52 (2) (2022) 425–461.
[12] K.I. Ozoemena, Z. Zhao, T. Nyokong, Immobilized cobalt (II) phthalocyanine–cobalt (II) porphyrin pentamer at a glassy carbon electrode: Applications to efficient amperometric sensing of hydrogen peroxide in neutral and basic media, Electrochem. Commun. 7 (2005) 679–684.
[13] Z. Bıyıklıoğlu, M. Durmuş, H. Kantekin, Tetra-2-[2-(dimethylamino)ethoxy]ethoxy substituted zinc phthalocyanines and their quaternized analoques: synthesis, characterization, photophysical and photochemical properties, J. Photochem. Photobiol. A Chem. 222 (1) (2011) 87–96.
[14] Z. Bıyıklıoğlu, M. Durmuş, H. Kantekin, Synthesis, photophysical and photochemical properties of quinoline substituted zinc (II) phthalocyanines and their quaternized derivatives, J. Photochem. Photobiol. A Chem. 211 (2010) 32–41.
[15] S.A. Znoiko, M.A. Serova, A.A. Uspenskaya, A. V. Zav'yalov, V. E. Maizlish, G. P. Shaposhnikov,, Nucleophilic substitution in 4-bromo-5-nitrophthalonitrile: XIV. Synthesis and properties of 4,5-bis[4-(1-methyl-1-phenylethyl)phenoxy]phthalonitrile and phthalocyanines therefrom, Russ. J. Gen. Chem. 86 (11) (2016) 2501–2507.
[16] D.D. Perrin, W.L.F. Armarego, Purification of laboratory chemicals, 2nd ed., Pergamon Press, Oxford, 1989.
[17] V. Cakir, F. Demir, Z. Biyiklioglu, A. Koca, H. Kantekin, Synthesis, characterization, electrochemical and spectroelectrochemical properties of metal-free and metallophthalocyanines bearing electropolymerizable dimethylamine groups, Dyes Pigment. 98 (2013) 414–421.
[18] S. Unlu, M.N. Yarasir, M. Kandaz, A. Koca, B. Salih, Synthesis, spectroscopy and electrochemical properties of highly soluble fluoro containing phthalocyanines, Polyhedron 27 (2008) 2805–2810.
[19] T. Nyokong, Electronic spectral and electrochemical behavior of near infrared absorbing metallophthalocyanines, Funct. Phthalocyanine Mol. Mater. (2010) 45–87.
[20] J.C. Swarts, E.H. Langner, N. Krokeide-Hove, M.J. Cook, Synthesis and electrochemical characterisation of some long chain 1, 4, 8, 11, 15, 18, 22, 25-octa-alkylated metal-free and zinc phthalocyanines possessing discotic liquid crystalline properties, J. Mater. Chem. 11 (2001) 434–443.
[21] S. Altun, A.R. Özkaya, M. Bulut, Peripheral octa-substituted metal-free, cobalt (II) and Zinc (II) phthalocyanines bearing coumarin and chloro groups: Synthesis, characterization, spectral and electrochemical properties, Polyhedron 48 (2012) 31–42.
[22] H.T. Akçay, R. Bayrak, Ü. Demirbaş, A. Koca, H. Kantekin, I. Değirmencioğlu, Synthesis, electrochemical and spectroelectrochemical properties of peripherally tetra-imidazole substituted metal free and metallophthalocyanines, Dyes Pigment. 96 (2013) 483–494.
[23] A. Koca, A.R. Özkaya, Y. Arslanoğlu, E. Hamuryudan, Electrochemistry, spectroelectrochemistry and electrochemical polymerization of titanylphthalocyanines, Electrochim. Acta 52 (2007) 3216–3221.
[24] G. Mbambisa, P. Tau, E. Antunes, T. Nyokong, Synthesis and electrochemical properties of purple manganese (III) and red titanium (IV) phthalocyanine complexes octa-substituted at non-peripheral positions with pentylthio groups, Polyhedron 26 (2007) 5355–5364.
[25] F. Demir, A. Erdoğmuş, A. Koca, Titanyl phthalocyanines: Electrochemical and spectroelectrochemical characterizations and electrochemical metal ion sensor applications of Langmuir films, J. Electroanal. Chem. 703 (2013) 117–125.
[26] A.M. Sevim, H.Y. Yenilmez, M. Aydemir, A. Koca, Z.A. Bayır, Synthesis, electrochemical and spectroelectrochemical properties of novel phthalocyanine complexes of manganese, titanium and indium, Electrochim. Acta 137 (2014) 602–615.
[27] A.B.P. Lever, P.C. Minor, J.P. Wilshire, Electrochemistry of manganese phthalocyanine in nonaqueous media, Inorg. Chem. 20 (8) (1981) 2550–2553.
[28] J. Obirai, N.P. Rodrigues, F. Bedioui, T. Nyokong, Synthesis, spectral and electrochemical properties of a new family of pyrrole substituted cobalt, iron, manganese, nickel and zinc phthalocyanine complexes, J. Porphyrins Phthalocyanines 07 (07) (2003) 508–520.
[29] N. Sehlotho, M. Durmuş, V. Ahsen, T. Nyokong, The synthesis and electrochemical behaviour of water soluble manganese phthalocyanines: anion radical versus Mn (I) species, Inorg. Chem. Commun. 11 (5) (2008) 479–483.
[30] A. Koca, Spectroelectrochemistry of phthalocyanines, Electrochemistry of N4 Macrocyclic Metal Complexes, in: J.H. Zagal, F. Bedioui (Eds.), Electrochemistry of N4 Macrocyclic Metal Complexes, Springer International Publishing, Cham, 2016, pp. 135–200.
[31] İ. Özçeşmeci, A. Koca, A. Gül, Synthesis and electrochemical and in situ spectroelectrochemical characterization of manganese, vanadyl, and cobalt phthalocyanines with 2-naphthoxy substituents, Electrochim. Acta 56 (2011) 5102–5114.
[32] D. Arıcan, M. Arıcı, A.L. Uğur, A. Erdoğmuş, A. Koca, Effects of peripheral and nonperipheral substitution to the spectroscopic, electrochemical and spectroelectrochemical properties of metallophthalocyanines, Electrochim. Acta 106 (2013) 541–555.
[33] Z. Jin, K. Nolan, C. McArthur, A. Lever, C. Leznoff, Synthesis, electrochemical and spectroelectrochemical studies of metal-free 2, 9, 16, 23-tetraferrocenylphthalocyanine, J. Organomet. Chem. 468 (1994) 205–212.
[34] A. Alemdar, A.R. Özkaya, M. Bulut, Synthesis, spectroscopy, electrochemistry and in situ spectroelectrochemistry of partly halogenated coumarin phthalonitrile and corresponding metal-free, cobalt and zinc phthalocyanines, Polyhedron 28 (2009) 3788–3796.
[35] A. Koca, A.R. Özkaya, M. Selçukoğlu, E. Hamuryudan, Electrochemical and spectroelectrochemical characterization of the phthalocyanines with pentafluorobenzyloxy substituents, Electrochim. Acta 52 (2007) 2683–2690.
[36] P. Tau, T. Nyokong, Synthesis and electrochemical characterisation of α-and β-tetra-substituted oxo (phthalocyaninato) titanium (IV) complexes, Polyhedron 25 (2006) 1802–1810.
[37] D. Quinton, E. Antunes, S. Griveau, T. Nyokong, F. Bedioui, Cyclic voltammetry and spectroelectrochemistry of a novel manganese phthalocyanine substituted with hexynyl groups, Inorg. Chem. Commun. 14 (2011) 330–332.
[38] C.-L. Lin, C.-C. Lee, K.-C. Ho, Spectroelectrochemical studies of manganese phthalocyanine thin films for applications in electrochromic devices, J. Electroanal. Chem. 524 (2002) 81–89.
[39] I. Yilmaz, In situ monitoring of metallation of metal-free phthalocyanine via UV-Vis and steady-state fluorescence techniques. Thin-layer UV-Vis and fluorescence spectroelectrochemistry of a new non-aggregating and electrochromic manganese (3+) phthalocyanine, New J. Chem. 32 (2008) 37–46.
[40] B. Agboola, K.I. Ozoemena, P. Westbroek, T. Nyokong, Synthesis and electrochemical properties of benzyl-mercapto and dodecyl-mercapto tetrasubstituted manganese phthalocyanine complexes, Electrochim. Acta 52 (2007) 2520–2526.
[41] S.G. Feridun, E.B. Orman, Ü. Salan, A.R. Özkaya, M. Bulut, Synthesis, characterization, and electrochemical and in-situ spectroelectrochemical properties of novel peripherally and non-peripherally 7-oxy-3-(3, 4-dimethoxyphenyl) coumarin substituted phthalocyanines, Dyes Pigment. 160 (2019) 315–327.
[42] S. Altun, Z. Odabaş, A. Altındal, A.R. Özkaya, Coumarin-substituted manganese phthalocyanines: synthesis, characterization, photovoltaic behaviour, spectral and electrochemical properties, Dalton Trans. 43 (2014) 7987–7997.
[43] V. Çakır, F. Demir, Z. Bıyıklıoğlu, A. Koca, H. Kantekin, Synthesis, characterization, electrochemical and spectroelectrochemical properties of metal-free and metallophthalocyanines bearing electropolymerizable dimethylamine groups, Dyes Pigment. 98 (2013) 414–421.
[44] D. Akyüz, T. Keleş, Z. Biyiklioglu, A. Koca, Electrochemical pesticide sensors based on electropolymerized metallophthalocyanines, J. Electroanal. Chem. 804 (2017) 53–63.
[45] J. Obirai, T. Nyokong, Synthesis, spectral and electrochemical characterization of mercaptopyrimidine-substituted cobalt, manganese and Zn (II) phthalocyanine complexes, Electrochim. Acta 50 (2005) 3296–3304.
[46] Ü.E. Özen, T. Keleş, Z. Bıyıklıoğlu, A. Koca, A. Rıza Özkaya, Electropolymerization and electrochemical pesticide sensor application of metallophthalocyanines bearing polymerizable morpholin groups, J. Electrochem. Soc. 163 (14) (2016) B673–B682.